Electronic Journal of University of Aden for Basic and Applied Sciences
EJUA-BA Vol. 3 No. 3 (2022)
https://doi.org/10.47372/ejua-ba.2022.3.178
ISSN: 2708-0684

RESEARCH ARTICLE

TUNING THE STRUCTURAL, OPTICAL AND PHOTOVOLTAIC CHARACTERISTICS OF FABRICATED N-TIO_2/P-CUO AND N-TIO_2/P-CU_2O SOLAR CELLS BY CHANGING THE BACK CONTACT ELECTRODES

M. A. Dabban[1,*] and Ammar Qasem[2]

[1] *Department of Physics, Faculty of Science, University of Aden, Aden, P.O. 6312, Yemen*
[2] *Department of Physics, Faculty of Science, Al-Azhar University, Nasr City 11884, Cairo, Egypt*

***Corresponding author: M. A. Dabban; E-mail: mehdi.ahmed.scie@aden-univ.net**

Received: 09 July 2022 / Accepted: 21 July 2022 / Published online: 30 September 2022

Abstract

The current work focuses on working a comparison between two solar cells made with the combination, *n*-TiO_2/p-CuO, and *n*-TiO_2/p-Cu_2O devices. The structural, optical, and photovoltaic characteristics were detailed. In the optical section, the optical measurements for the TiO_2 (120 *nm*), CuO (200 *nm*), and Cu_2O (200 *nm*) thin films were illustrated, and then the energy of optical transition was calculated based on the Tauc formula for each layer. The direct optical gap energies of TiO_2, CuO, and Cu_2O thin films are 3.24, 1.77, and 2.18 eV, respectively. The front contact electrode in both systems is an ITO- coated glass layer, while the back contact electrodes are Pt, Ni, Au, Co, Ag, Cu, Al, and Mo. The effect of various metals as back contact electrodes on the photovoltaic characteristics of fabricated devices was investigated. The optical and structural characteristics showed the superiority of the fabricated device n-TiO_2/p-CuO over the fabricated device n-TiO_2/p-Cu_2O.

Keywords: Thin Films, Optical parameters, n-TiO_2/ p-CuO and n-TiO_2/ p-Cu_2O Solar Cells.

1. Introduction

Generally, photovoltaic (PV) systems are valuable sustainable energy resources that have the ability to address a variety of worldwide energy problems [1]. The demand for modern energy systems is increasing day by day as all deployed PV systems in the world had a capacity of 480 GW by the end of 2018 [2]. Enhancing the performance of photovoltaic (PV) devices is a crucial goal that can be achieved by utilizing basic semiconductor materials such as metal oxides. The majority of these oxides are non-toxic, chemically steady, plentiful, and low-cost [2-4]. Metal oxides physical and chemical properties must be specified, explained, and understood for this reason, as well as because they are increasingly used in technology [5-7].

Since copper is multivalent, it can form a number of oxides, including copper oxide CuO and copper dioxide (Cu_2O). These two oxides have distinct characteristics, such as color, surface morphology, and the majority of their physical properties. Because of their appropriate electrical and optical characteristics both oxides are being used as potential candidates for photovoltaic devices. On the other hand, the bandgap of copper dioxide (Cu_2O) is 2 eV, which is within a suitable window material range, while, the bandgap of copper oxide (CuO) is 1.2 eV. This value is making it an ideal absorber for photonic devices [8, 9]. In general, Copper oxide crystallizes and solidifies in 2 types: cupric oxide which recognized as tenorite (CuO), and cuprous oxide, also identified as cuprite (Cu_2O). The bandgap of the tenorite (CuO) type is between 1.1 and 1.9 eV, and it has a monoclinic structure, while the bandgap of the cuprite (Cu_2O) type is between 2.1 and 2.6 eV, and it has a cubic structure. Cu deficient CuO, as well as the copper that is abundant with oxygen (Cu_2O), demonstrate original p-type conductivity owing to copper vacancies in the monoclinic and cubic structures for such types [10, 11].

CuO and Cu_2O thin films are commonly utilized in a range of applications, including light-emitting diodes, energy storage cells, thin-film transistors, super capacitors, infrared detectors, photovoltaic devices, and

optical stability control, among others [12-16]. CuO thin films could also be used in solar cells, photo sensor systems, photo catalytic techniques, and elevated superconducting compounds [17-19]. Furthermore, CuO compounds were also used in diode devices, lithium-copper oxide electrochemical modules and field emission systems, among other applications [14, 17-19]. On the other side, owing to the variation in the electrical conductivity caused by the reaction of the gas with the oxygen adsorbed on the surface, copper oxide-based sensors have many uses in the production of gas sensing instruments [20, 21].

Vacuum annealing for the CuO thin film utilizing the standard techniques such as pulsed laser deposition [12], chemical vapor deposition [22], and magnetron sputtering [23], *etc*, could generate the Cu_2O thin film. There were many studies on annealing CuO in air or vacuum to produce the Cu_2O compound, such as an annealing of the CuO sample in a vacuum at 500°C. This process was improved the optical transmittance in the visible region of the spectrum by 55% and improved the electrical performance, thereby increasing the mobility of the charges to 47 cm^2/Vs[24].

There were several methods for preparing copper oxide and copper dioxide where the CuO thin films were also generated utilizing a variety of techniques, including sol-gel pathway [25], and microwave technique [26], etc. On the other hand, there are several methods and techniques for preparing Cu_2O and depositing it in form of thin films as indicated by the corresponding references [27-31]. However, among these techniques, several works were reported in which Cu_2O was prepared by the method of electrodeposition [32-35]. Such last approach is appealing due to its flexibility, low cost, and low-temperature procedure; on the other side, the material's composition could be easily fixed, resulting in changes in physical properties. Although CuO and Cu_2O are critical as absorbent layers in solar cells, the yield and efficiency of the solar cell are not solely dependent on these two oxides; rather, the yield and properties of the solar cell are dependent on the contact electrodes being ohmic and having a broad working function. The energy required to extract electrons from a solid to a point completely outside the solid surface in a vacuum is called the metal work function [36]. As well, the CuO and Cu_2O layer are widely used in photovoltaic and solar cell systems [37, 38].

Briefly, a p–n junction is formed when a Cu_2O layer is placed on a TiO_2 layer. On the other hand, the heterojunction generated by meeting TiO_2 and CuO layers is a promising contender for photovoltaic (PV) and photocatalytic applications [39]. As previously stated, the layers of Cu_2O and CuO are acted as absorber layers and are p-type solar cell materials with tiny, direct band gaps extending from 2.0 to 2.6 eV for the Cu_2O layer [10] and 1.0 to 2.1 eV for the CuO layer [11]. TiO_2 layer acts as an n-type semiconductor with gap energy of more than 3 eV in heterojunction systems and for this reason, the TiO_2 layer in these devices is used as a buffer (window layer) [1]. As well, the TiO_2 layer is well-known for its numerous functions and potential as a dye-sensitized solar cell material [1,39]. Despite the fact that a variety of TiO_2/Cu_2O and TiO_2/CuO solar cells have been constructed in a variety of methods, the energy conversion efficiency of TiO_2/Cu_2O heterojunction is less than 2%, and TiO_2/CuO heterojunction is less than 20% [40-42].

The main impetus for this work is a very important one that benefits all researchers in the field of solar cells, photovoltaic detectors, and other photovoltaic devices. The current work focuses on the pivotal role that front and rear contact electrodes play in controlling the properties of fabricated solar cells, which is unknown to many researchers. The research focused on how to control the photoelectric properties of two fabricated solar cells by controlling the back contact electrodes of these two devices, and the secret lies in the change of properties to the difference in the work function of the metal used as the back contact electrode, where the importance of the work function of the metal lies in controlling the electrons emitted from the surface of the metal and thus controlling the total current passing through the fabricated device. Therefore, the current study is a continuation of previous research, but it focuses on two fabricated devices, n-TiO_2/p-CuO and n-TiO_2/p-Cu_2O, at the same time to demonstrate the characteristics of each fabricated device in dark and light conditions at different back contact electrodes (Pt, Ni, Au, Co, Ag, Cu, Al, and Mo), as well as one front contact electrode, ITO. Structural and optical properties with energy diagrams of the layers comprising the two fabricated devices are included to support the study.

2. Experimental Methodology

The heterojunctions with the traditional structure of (glass/ITO/n-TiO_2/p-Cu_2O/metal back contact) and (glass/ITO/n-TiO_2/p-Cu_2O/metal back contact) were fabricated as shown in **Fig. 1**. In such a system, Cu_xO (x=1 or 2) layer (200 *nm*) was deposited on TiO_2 thin layer (120 *nm*). The TiO_2 thin layer (120 *nm*) was deposited on the Indium tin oxide (ITO)-coated glass substrate (~2 *mm*). Utilizing a DC alignment and a two-electrode device, a titanium dioxide, TiO_2 layer was electrically deposited on indium tin oxide ITO-coated glass substrate while the (Pt, Ni, Au, Co, Ag, Cu, Al, and Mo) were connected to the Cu_xO (x=1 or 2) layer (200 *nm*).

The deposition bath of the TiO_2 layer was carried out in a mixed chemical solution of Titanyl sulfate, $TiOSO_4$ and oxalic acid, $C_2H_2O_4$ with molar concentrations equal to 0.01 M and 0.02 M for both compounds, respectively in a 100 ml beaker. By introducing 18 MΩ Millipore water

to the beaker, the final volume was raised to 100 ml. Then, a transparent solution was obtained, which was composed of a compound called bis(oxalato)oxo-titanate (IV) with the chemical formula [$TiO(COO)_2$]. Finally, using the described electrochemical deposition bath, the TiO_2 layer was deposited to the required thickness on direct ITO-coated glass substrate which pre-washed with soap solution, distilled water and then dipped for 5 *min.* in chromic acid in a beaker to remove the adhesive impurities on it. In order to thoroughly remove the impurities, the glass substrates were boiled in Millipore water and then acetone at the end of the stage before the start of chemical deposition. The back contact electrode was changed each time with one of the metals used as the back contact electrode (Pt, Ni, Au, Co, Ag, Cu, Al, and Mo). The back contact electrode was of high purity (~ 99.999 %) in the form of foil with a thickness of 100 *nm* contacted with the positive electrode of DC bias voltage to act as an anode while the glass substrate was externally contacted with the negative terminal of the DC bias voltage to act a cathode. The positive and negative electrodes were placed in the working solution to complete the preparation of the chemical preparation cell. The deposition process was performed out at 1.4 V and 298 K in an unstirred aqueous solution. On the other hand, the deposition material was done in the air for a 15 *min*. at 923 K to generate the anatase phase for the TiO_2 layer with a color yellowish white. The thickness of the studied films was measured utilized the quartz crystal monitor type (FTM4, Edwards). The CuO and Cu_2O layer were obtained using targets made from metal Cu in an atmosphere that contained a combination of highly pure argon Ar and oxygen O_2 with a purity level up to 99.999 % for each element. The deposition chamber pressure value was less than 3.75 $x10^{-6}$ Torr. The studied solar cells were made by adhering to the metal contacts (Pt, Ni, Au, Co, Ag, Cu, Al, and Mo) with silver conductive glue as the back contact, which was directly connected to the Cu_xO layer, and the ITO layer as the front contact. The thickness of the back and front contact was 100 *nm*.

The transmittance, *T*, and reflectance, *R*, were measured utilizing a double-beam spectrophotometer (Jasco V670) at normal incidence of light in the wavelength range between 300 and 2500 *nm*. At room temperature, by irradiating the bottom side of ITO layer utilizing the light beam coming from the glass, under dark and illuminated conditions (800mW/cm^2), the current density-voltage (*J-V*) characteristics of devices were measured with Keithley 610 C device. Utilizing an X-ray diffractometer (Philips type PW 1710 with Cu as a target and Ni as a filter, λ=1.5418 Å), the structural nature of the as-prepared thin layers was determined. The XRD data were measured for phase angle, 2θ between 15° and 120° with a scanning step and speed of 0.02°, and 0.06 °/s, respectively. The voltage and current applied to the tube are 40 kV and 25 mA, respectively. Scanning electron microscopy device with type Jeol-((JSM)-T200) was used to analyze the surface morphology of the studied layers. The chemical composition of the films was measured using the standard Energy-Dispersive X-ray (EDX) spectroscopy unit attached to the used electron microscope.

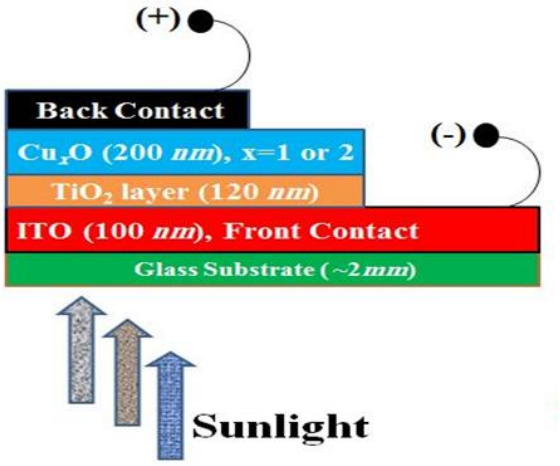

Fig. 1: Structure diagram of two fabricated devices.

3. Results and discussion

3.1 Structural maps

(EDX) analysis of the first fabricated device, namely, TiO_2/CuO is portrayed in **Fig. 2** for an example. This technique shows the consistency of the proportions of the elements in the bulk material and the samples in form of thin layers. The elemental analysis was carried out the presence of Ti, Cu and O and there aren't any other foreign elements other than our material. On the other hand, the SEM profile of the cross-section of the fabricated devices, glass/ITO/TiO_2/CuO, and glass/ITO/TiO_2/Cu_2O is incarnated in **Fig. 3 (a, b)**, respectively. A transparent mesoporous layer of TiO_2 (120 *nm*) and a scattering layer of CuO and Cu_2O (200 *nm*) are observed. EDS chemical maps incarnate the distribution of the different elements on the photoelectrode as embodied in **Fig. 4**. As expected, the titanium is homogeneously distributed on the film, while the oxygen signal is low on the left side of the ITO attributed to the silica on the glass substrate. Ti appears to be more concentrated in the inner titanium layer in the transparent film of TiO_2. Finally, it is observed that Cu is present in all the right layers, being a little more concentrated in the outer layer caused by the CuO and Cu_2O deposition method, depending on the particles' diffusion capacity. EDS mapping suggests that the larger particles are trapped in the pores near the surface of the film. At the same time, the little ones penetrate deeper into the film.

From another perspective, **Fig. 5 (a, b)** shows the results of examining the fabricated devices using the X-ray technique. Both figures show the distribution of the components of the fabricated devices in terms of the

phase angle. **Fig. 6 (a, b)** shows the distribution of Miller indices as a function of the spectral scatter angle of the two fabricated devices. From this figure, it is evident that the high Miller indices are found in the high spectral scattered regions. On the other side, the distance between atomic planes that provide diffraction peaks is called the d-spacing. The corresponding d-spacing is associated with each peak in the diffraction pattern. The atomic plane forms a three-dimensional coordinate system, which can be defined as a crystal path. The d-spacing's path in terms of phase scattering angle (the angle between the incident beam and the scattering plane) is illustrated in **Fig. 7 (a, b)** for both fabricated devices. Its relationship with phase angle appears to be a decreasing relationship in both fabricated devices.

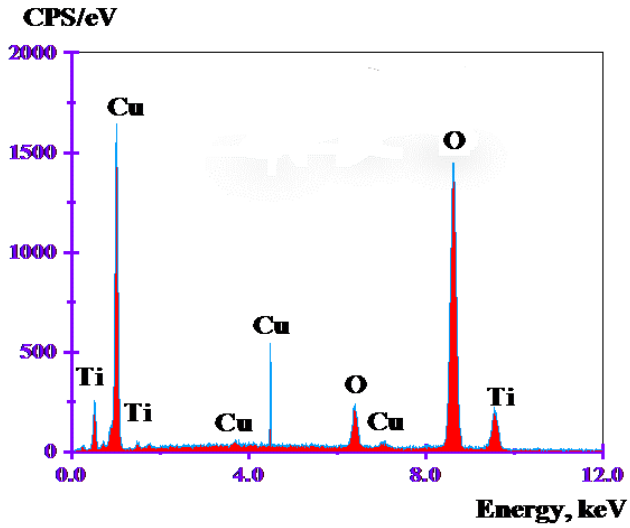

Fig. 2: EDX analysis of the first fabricated device, TiO_2/CuO.

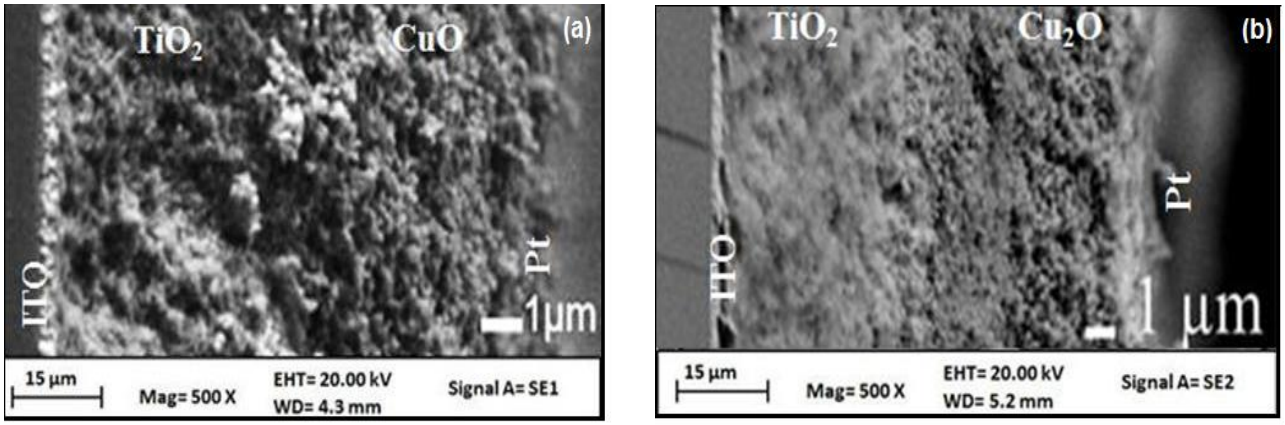

Fig. 3: Cross-section of the fabricated devices: **(a)** glass/ITO/TiO_2/CuO and **(b)** glass/ITO/TiO_2/Cu_2O.

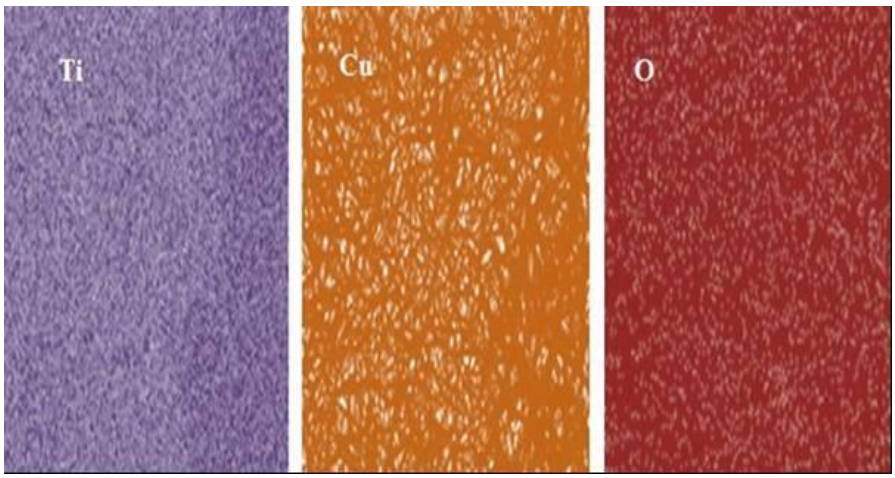

Fig. 4: EDS chemical maps incarnate the distribution of the different elements on the photo-electrode.

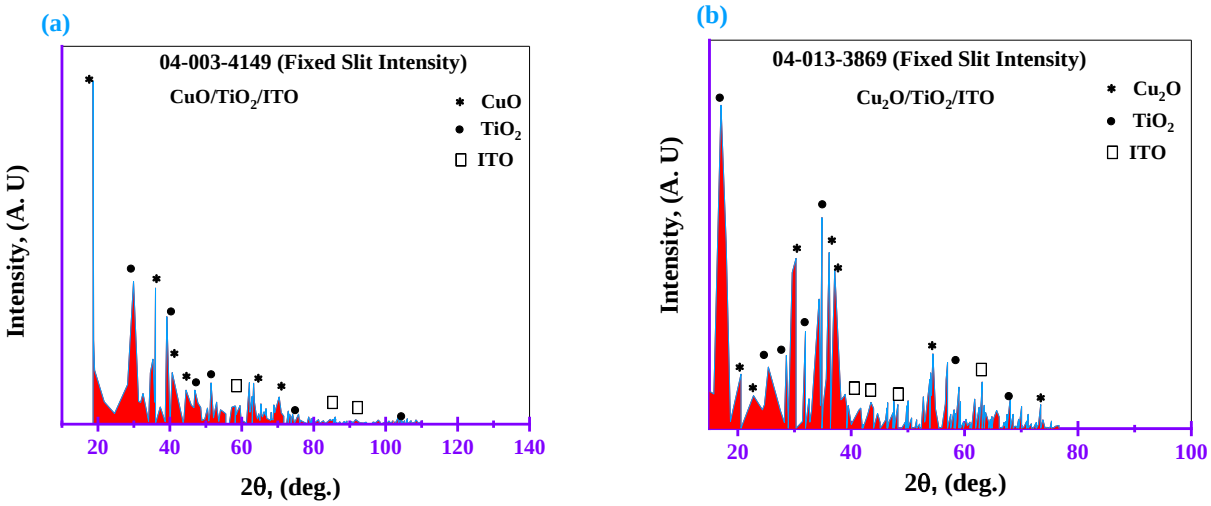

Fig. 5: X-ray check for the fabricated devices.

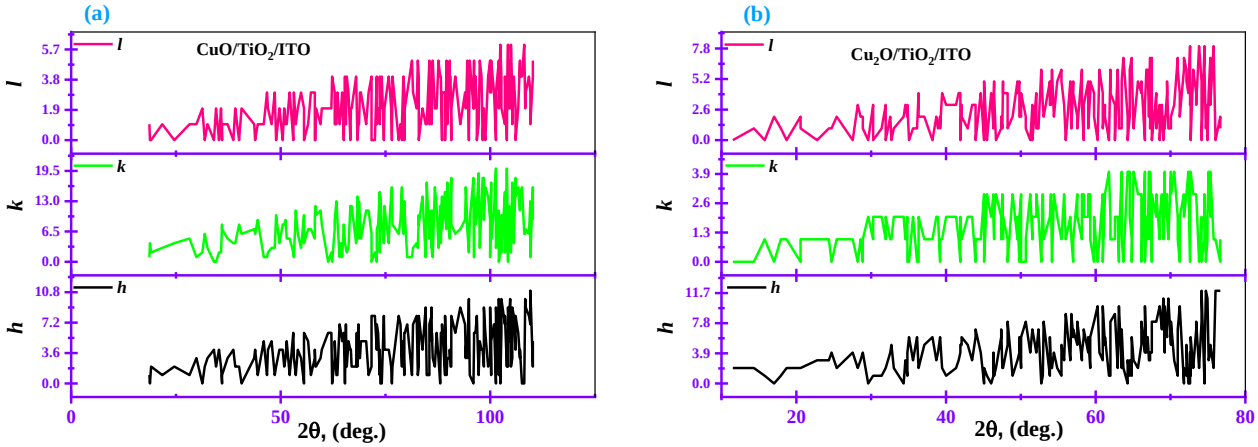

Fig. 6: The distribution of Miller indices as a function of the spectral scatter angle of the two fabricated devices.

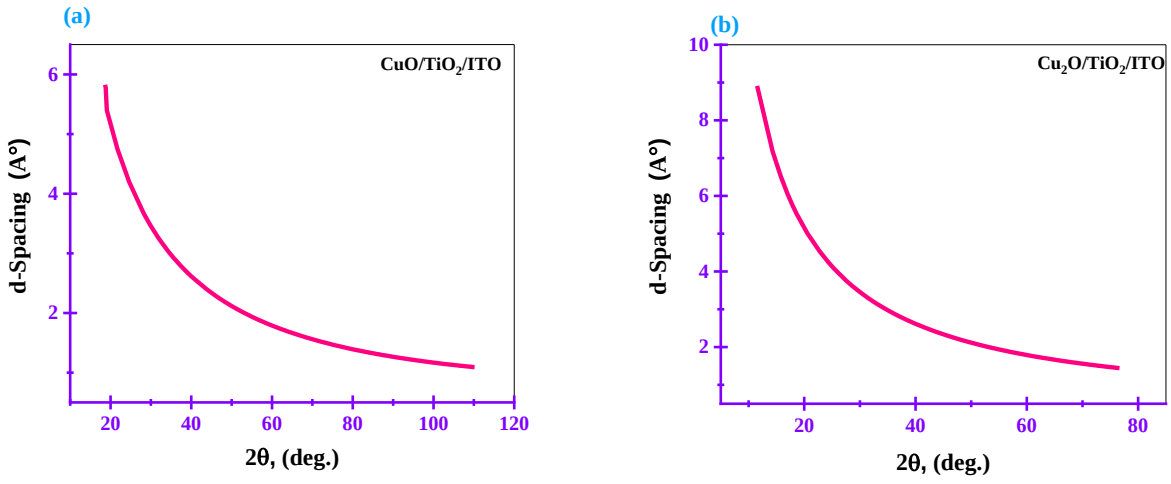

Fig. 7: d-Spacing as a function of the scattering angle for of the two fabricated devices.

3.2 X ray photon spectroscopy (XPS) analysis

To explain the chemical part of fresh CuO and Cu_2O (namely, the CuO which annealed at 500 K in vacuum) thin films and also to determine the valence state of copper, Cu, the X-ray photon spectroscopy (XPS) was utilized. To achieve this, the optical photon spectroscopy was used using X-rays via a radiation source with energy of 1490.4 eV on both oxides. The findings of this investigation contributed to the exploration of copper ions as well as the binding energy of both oxides (see **Fig. 8 (a, b)**).

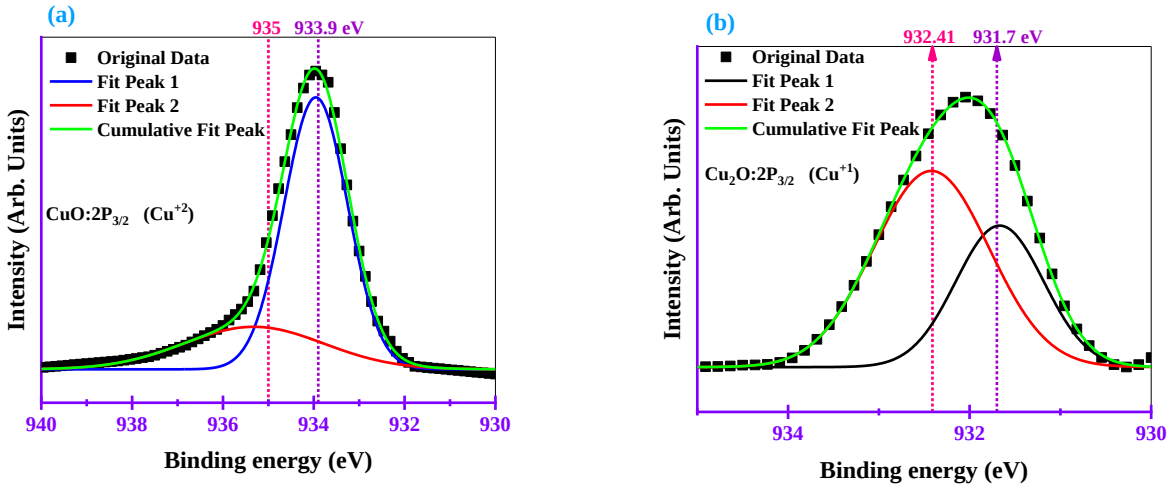

Fig. 8: The X-ray photon spectroscopy (XPS) of CuO and Cu_2O layers.

3.3 Optical aspects

3.3.1 The optical measurements and Tauc energy

In the spectral range between 300 and 2500 *nm*, **Fig. 9** depicts the transmittance and reflectance spectra of TiO_2 (120 *nm*), Cu_2O (200 *nm*) and CuO (200 *nm*) layers. As shown in Fig. 9, the changes in the optical transmission of layers show the shifts of the high energy absorption edges to higher wavelengths for TiO_2 (120 *nm*), Cu_2O (200 *nm*) and CuO (200 *nm*) layers, respectively. On the other hand, the optical gap energy E_g for all layers of the solar cell under study was determined using the Tauc equation-in the strong absorption region ($\alpha > 10^4$ cm^{-1}) described below [43-45] (see **Fig. 10**):

$$(\alpha.h\nu) = C.(h\nu - E_g)^r \quad (1)$$

In this equation, C incarnates an optical constant, $h\nu$ portrays the photon energy and α represents the absorption coefficient in terms of the optical measurements (*T*, *R*) and the thickness (*d*) of each layer. This quantity is computed by the listed below formula [45-48]:

$$\alpha(\lambda) = (d)^{-1}.\ln[\left((1-R)^2 + \sqrt{\{(1-R)^4 + 4(RT)^2\}}\right).\left(\frac{1}{2T}\right)] \quad (2)$$

The determined direct gap energy values for TiO_2 (120 *nm*), CuO (200 *nm*), and Cu_2O (200 *nm*) layers are arranged in the following order: 3.24, 1.77 and 2.18 eV, respectively. Energies of the three layers correspond to the energies of these layers which have been determined in previous studies and are included in the corresponding references [37-42, 48].

In a related context, the energy positions of the studied devices are computed utilizing the following equations [48]:

$$E_{CB} = E_C - \chi + \left(0.5E_g\right) \quad (3)$$

$$E_{VB} = E_C - \chi - \left(0.5E_g\right) \quad (4)$$

$$\chi(A_xB_y) = \left(\left(\frac{E_{EA} + E_{Ion}}{2}\right)_A^x . \left(\frac{E_{EA} + E_{Ion}}{2}\right)_B^y\right)^{\frac{1}{x+y}} \quad (5)$$

Here: E_{EA} incarnates the electron affinity, E_{Ion}. portrays the ionization energy, and E_g refers to the bandgap energy for each layer as we mentioned. The obtained values of E_{EA} and E_{Ion} : for *Ti* are 0.075 and 6.830 eV [49], E_{EA} and E_{Ion} for O are 1.461and 13.621 eV [50] and these quantities for Cu are 1.235 and 7.729 eV, respectively [51]. On the other hand, the value of E_C is an energy constant and equals to 4.5 eV [52, 53]. The energy positions of the TiO_2, CuO, and Cu_2O layers are illustrated in **Fig. 11 (a, b)** depending on the above equations and mentioned values.

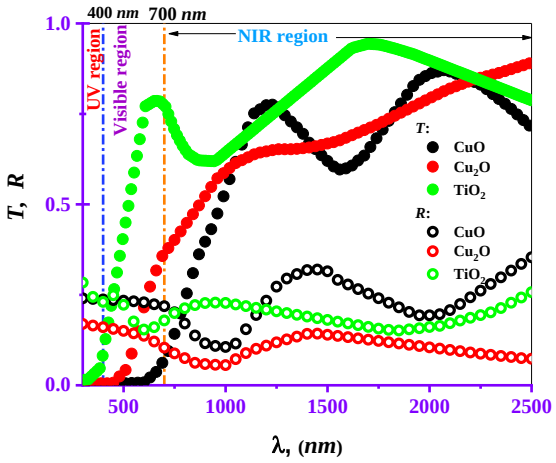

Fig. 9: The transmittance and reflectance spectra of TiO_2 (120 *nm*), CuO (200 *nm*), and Cu_2O (200 *nm*) layers.

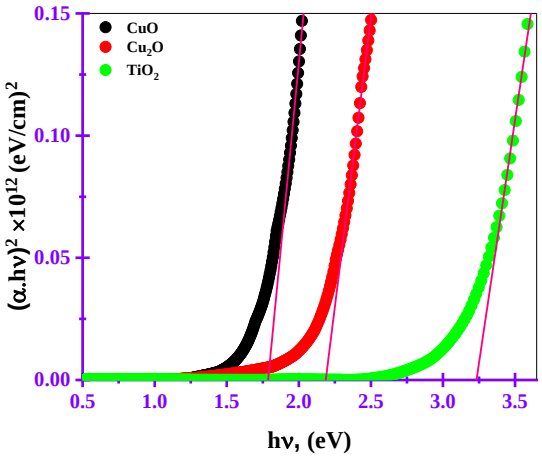

Fig. 10: The direct optical gap energy E_g according to Tauc equation in the strong absorption region.

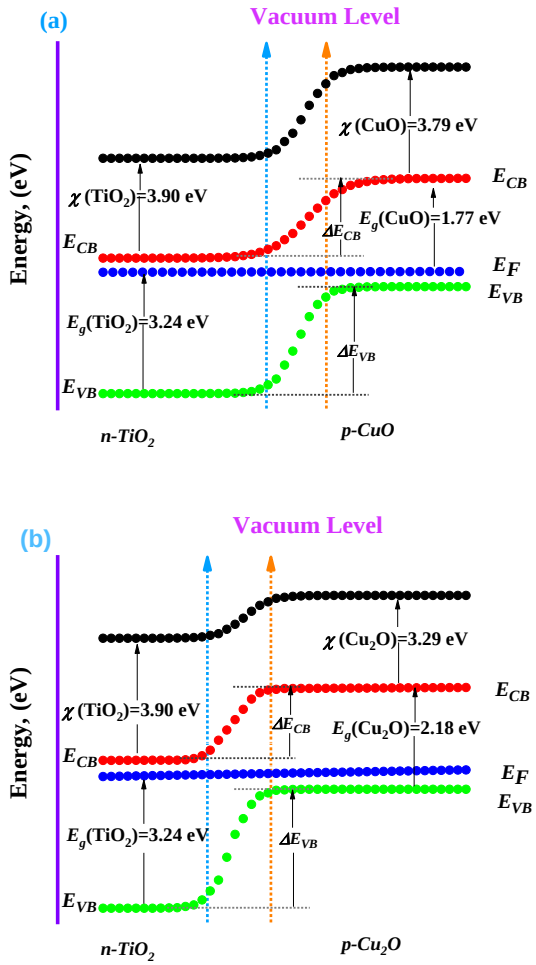

Fig. 11: The energy diagrams of the studied devices.

3.3.2 Dark (J-V) characteristics

In the range of (-2V to 2 V), **Fig. 12 (a, b)** highlights the current density as a function of the bias voltage (*J-V* characteristics) applied to the n-TiO_2/p-CuO solar cell at different back contact electrodes. On the other hand, **Fig. 13 (a, b)** presents the paths of current density behavior as a function of the applied voltage for the n-TiO_2/p-Cu_2O solar cell. The dark (*J-V*) characteristics are exceptionally beneficial in determining the transport mechanisms in the fabricated devices. The rectification behavior of the two devices is fully evident in the dark, and it is decreased when the back contact electrode is changed [54]. The curves are demonstrated diode behavior, with the forward path to the negative potential on the ITO-coated glass substrate. The creation of a p-n heterojunction, in which the boundary at the interface restricts forward and reverse carrier flow across the interface, where the built-in potential could be created, explains this behavior. The development of a depletion region between the ITO-coated glass substrate with n-TiO_2 film and a CuO or Cu_2O layer with a back contact electrode is due to the exponential dependency in the lower voltage range for both devices. It is worth noting here that the current density-voltage of the fabricated n-TiO_2/p-Cu_2O device is lower than that which describes the behavior of the generated n-TiO_2/p-CuO device. The ohmic and Schottky effects of both fabricated devices reflect the mechanisms for transporting charge carriers in the septum between the sides of the device.The reverse current density in two fabricated devices has a slight voltage dependency, and the demonstrated voltage dependence of the current density is greater than expected by pure thermal conduction or the Schottky phenomenon at higher reverse voltages. As a result, it's possible to suit essentially flat reverse (*J-V*) characteristics across a large voltage range, suggesting that carrier production and recombination in the ITO-coated glass substrate is the predominant source of reverse current density [55].

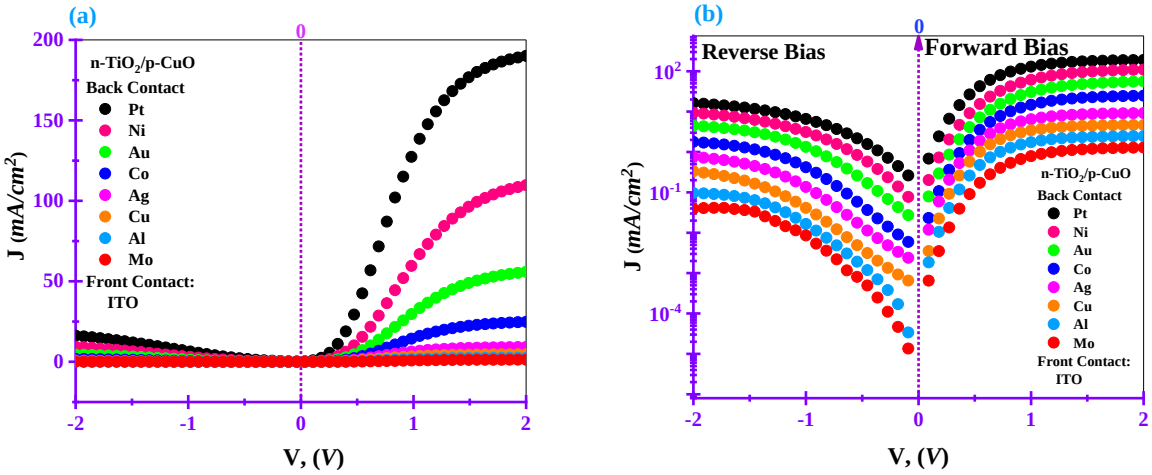

Fig. 12: The dark (current density-voltage) characteristics for the n-TiO$_2$/p-CuO solar cell.

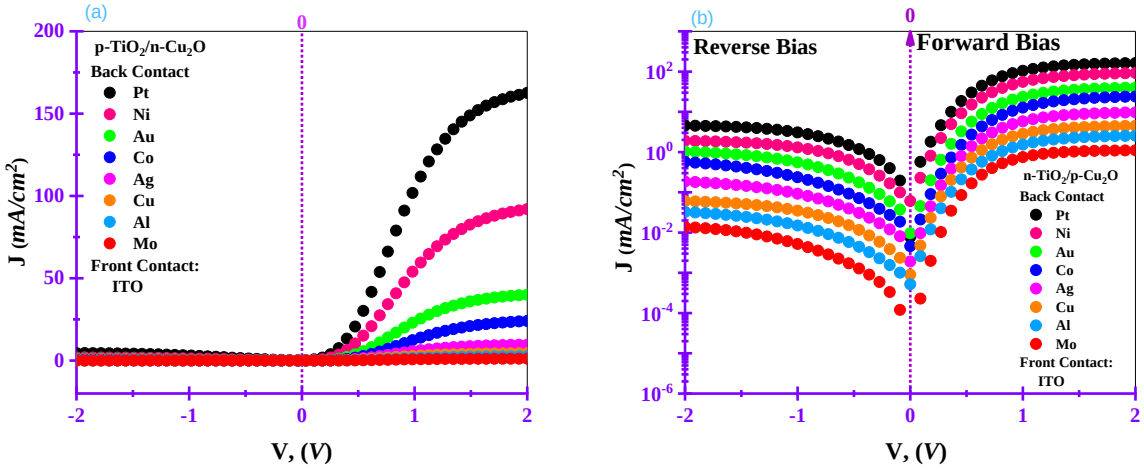

Fig. 13: The dark (current density-voltage) characteristics for the n-TiO$_2$/p-Cu$_2$O solar cell.

3.4 Illuminated (J-V) and (P-V) characteristics

3.4.1 Illuminated (J-V) characteristics

Illuminated (*J-V*) characteristics in the range between -2 and 2 V are extensively studied at different back contact electrodes, (Pt, Ni, Au, Co, Ag, Cu, Al, and Mo) and one front contact electrode represented by the ITO-coated glass substrate. The aforementioned study included both fabricated devices in this work. **Fig. 14 (a, b)** and **Fig. 15 (a, b)** highlight the illuminated (*J-V*) characteristics of both generated devices. It is clear from both figures the axial role of the back contact electrodes in controlling the circuit opening voltage of the solar cell, which is found to be decreased with decreasing the work function of the metal used as the back contact electrode. On the other hand, it is found that the values of short-circuit current density; J_{sc} is increased in all the fabricated devices. When the back contact electrode changes according to the work function, the value of short circuit current density is changed by around 2.5%. Since this value is so large, the effect of changing the back contact electrode on the short circuit current density can be noticed as long as the temperature and amount of solar radiation remain constant for all fabricated devices [56]. The metal does not form an oxide layer with the layers it fuses on as the work function of the metal increases. As a result, the work function for metal is the only parameter that is efficient in achieving the direction of reverse bending, in which the photo-generated holes can move freely and easily to the metal contact electrode while a Schottky barrier prevents electron transport. Since platinum has the highest work function and molybdenum has the lowest work function, the Schottky barrier is higher in platinum, Pt, and lowers in molybdenum, Mo, in the electrodes used in our current study. Consequently, the opening voltage in the case of metal with a high work function is higher and decreases with decreasing the work function of the metal contact electrode. It can now be said that the higher the work function of the metal, the higher the open-circuit voltage of the solar cell, and that the opposite happens only when a layer of metal oxide forms on the surface of the metal contact electrode and serves as a blocking layer. It is worth noting here that the circuit opening voltage of the n-TiO$_2$/p-Cu$_2$O solar cell is

lower than the circuit opening voltage of the n-TiO_2/p-CuO solar cell. This is due to the higher optical gap energy of Cu_2O (2.18 eV) compared to CuO (1.77 eV). This, in turn, makes it difficult for electrons to easily move between the valence and conduction bands, thus reducing the circuit opening voltage. Observed values for the open-circuit voltage of the two fabricated devices are included in **Table 1**.

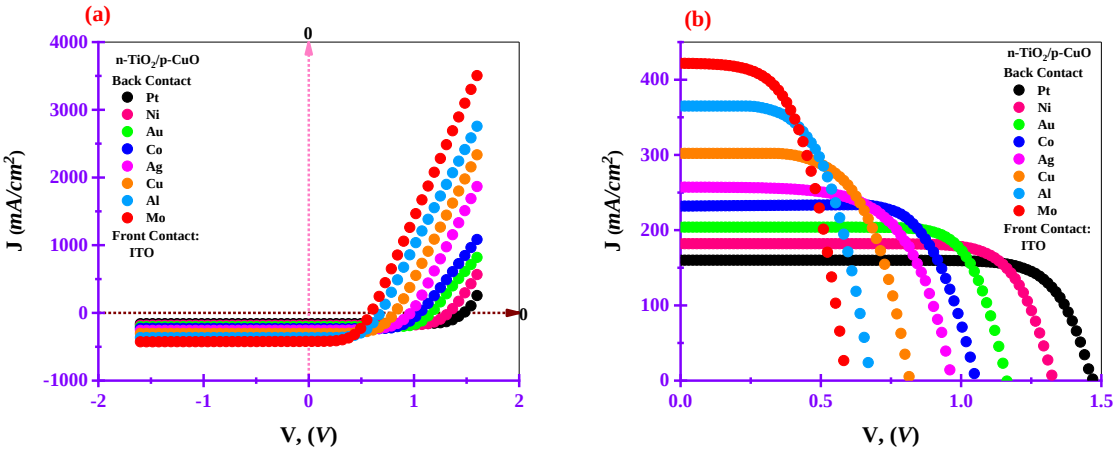

Fig. 14: (a, b) Illuminated (current density-voltage) characteristics for the n-TiO2/p-CuO solar cell.

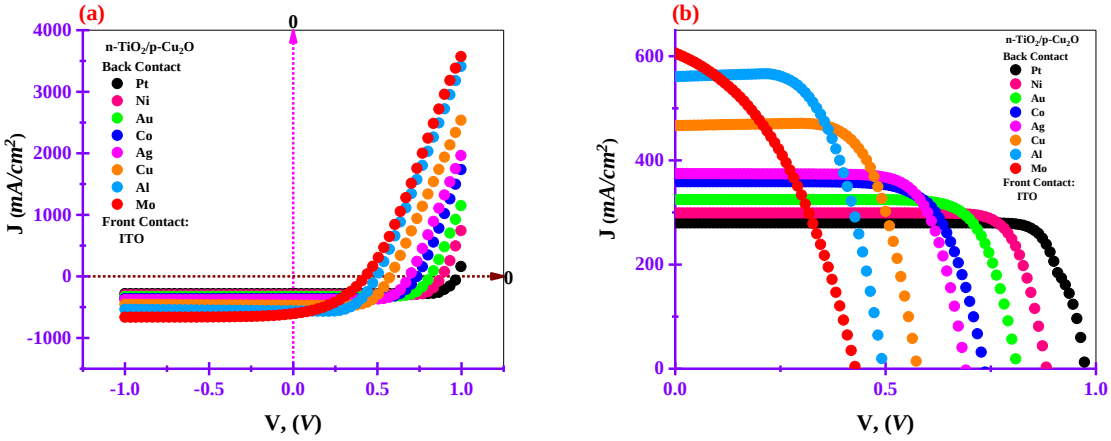

Fig. 15: (a, b) Illuminated (current density-voltage) characteristics for the n-TiO2/p-Cu2O solar cell.

3.4.2 Illuminated (P-V) characteristics

At an input power of $P_{in} = 800$ mW/cm^2 from a light source, the power-voltage characteristics of all the fabricated devices are illustrated in **Figs. 16** and **17**. Such figures reflect the illuminated (power-voltage, (*P-V*)) characteristics of n-TiO_2/p-CuO and n-TiO_2/p-Cu_2O solar cells in the positive bias (0- 2 V), respectively. The open-circuit voltage, V_{OC} and short-circuit current density, J_{SC} are the most critical parameters to obtain for both fabricated devices. After that, using the following equations [57] to calculate the power conversion efficiency (*PCE*) and the fill factor (*FF*):

$$PCE = \left(\frac{P_{\max}}{P_{in}}\right)\% \qquad (6)$$

$$FF = \left(\frac{V_{\max} . J_{\max}}{V_{OC} . J_{SC}}\right) = \frac{P_{\max}}{V_{OC} . J_{SC}} \qquad (7)$$

Here, $V_{\max}$, $J_{\max}$ and $P_{\max}$ are indicated the maximum values for voltage, current density, and output power, respectively. The calculated values for these quantities are listed in **Table 1**. It is evident from **Table 1** that *PCE* and *FF* for the n-TiO_2/p-CuO solar cell are higher than these quantities for the n-TiO_2/p-Cu_2O solar cell at different back contact electrodes. On the other hand, one can find that these two quantities decrease as decreasing the work function of the metal contact electrode used as the back electrode in both the fabricated solar cells. It is clear from the table that we were able to create solar cells with high power conversion efficiency (*PCE*) and high fill factor (*FF*). All of the two fabricated devices showed good characteristics, with the n-TiO_2/p-CuO device being more favorable than the n-TiO_2/p-Cu_2O device. On the other hand, fabricated solar cells of each type excel when the back contact electrode is platinum compared to other fabricated solar cells when using other back electrodes. The behavior of the parameters in the case of studying the characteristics in light for both fabricated

devices at different back contact electrodes is related to several factors that explained according to an experimental data and the general behavior of these parameters in other solar cells as follows:

1- The fill factor, *FF* is based on the following main variables:

- Since FF is used to measure the squareness of the (*J-V*) graph, a higher voltage solar cell will have a higher FF because the rounded portion of the (*J-V*) graph absorbs less energy [58].
- The energy conversion efficiency of *FF* is improved by minimizing incident light reflection [59].

2- The main determinants of open-circuit voltage are as follows:

- Potential difference between the hole transport layer and the electron transport layer, assuming that these layers make the role of ohmic contacts with the transport layer[60]. If it is non-ohmic, it will reduce the contact difference voltage, reducing solar cell performance [61]. As a result, the lower the back contact electrode's work function, the more the contact behavior shifts away from non-ohmic activity and toward the first behavior, also known as the Schottky barrier [62]. This, in turn, reduces the open-circuit voltage of the solar cell. On the other side, the contact potential difference has to be close to the energy difference between the acceptor's LUMO and the donor's HOMO levels. The LUMO level of the electron in the acceptor layer has to be lower than those of the donor absorber layer by an energy difference larger than the exciton depersonalization energy to distinguish the electrons and holes in the exciton[63, 64].
- In reality, when the photo current density is balanced by the dark current density, an open circuit is formed. Thus, in addition to selecting the best materials for the energy levels, high-quality layers must be used to avoid recombination [65].

3- The short circuit current density is related to the following main parameters:

- The active layer's absorption efficiency based on the front and back contact electrodes, which should be extremely efficient on the majority of wavelengths for fallen solar rays. Thus, if the absorption coefficient is higher, the photo-current density would be higher. We were able to achieve a reasonably constant value of short circuit current density by keeping the absorption coefficient of the layers attached to the two contact electrodes without high changed [66].
- The thickness of the absorber layers in the solar system is the second main factor which must be thick enough to absorb the incident solar radiation's highest cut-off wavelength [67]. This implies that the absorber layer has to be efficient and produce excitons in response to solar irradiation. The inner quantum efficiency of this factor measures its effectiveness. For this, we have made the thickness of the thin layers suitable enough to absorb the cut-off wavelengths and thus ensure that the value of short circuit current density remains close to each other.
- A solar cell's short-circuit current density is proportional to its light intensity (the number of photons). For this reason, the input power of both devices was standardized at different rear contact electrodes, where, $P_{in} = 800\ mW/cm^2$.
- The incident light spectrum was standardized at AM1.5 spectrum for both fabricated solar cells.

Finally, we found that a system with a CuO layer and a Pt-back contact electrode would work better as an absorber layer in solar cells during photo-conversion mechanisms.

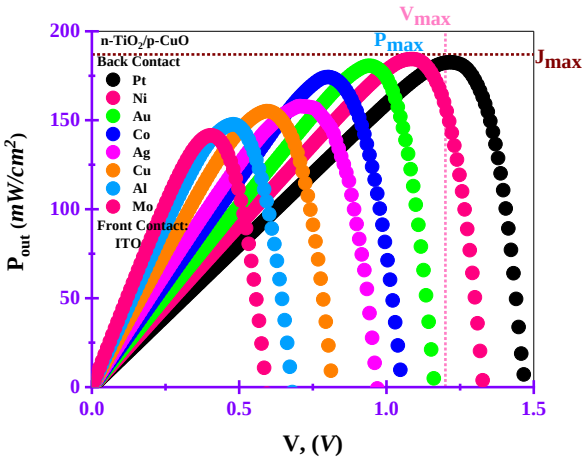

Fig. 16: The (Power-voltage) characteristics for the n-TiO$_2$/p-CuO solar cell.

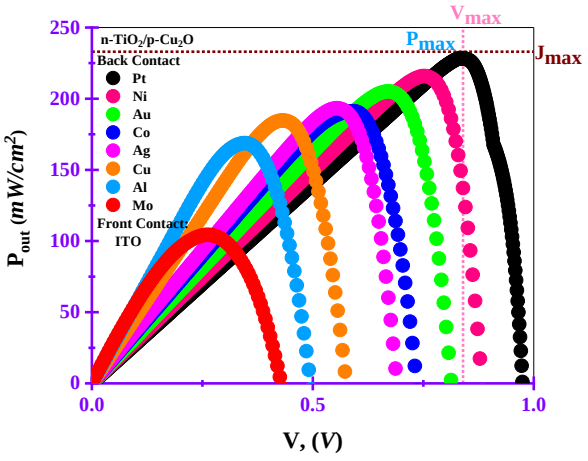

Fig. 17: The (Power-voltage) characteristics for the n-TiO$_2$/p-Cu$_2$O solar cell.

Table 1: Back contact electrodes, work function (WF) and illuminated parameters of fabricated solar cells.

The Solar cell	Back contact electrode		WF (eV)	Jsc (mA/cm2)	Voc (V)	Pmax (mW/cm2)	FF	PCE%
	Name	Symbol						
n-TiO2/p-CuO	Platinum	Pt	5.6	160.0	1.50	195.37	0.814	24.42
	Nickel	Ni	5.15	182.0	1.347	188.10	0.767	23.51
	Gold	Au	5.1	203.9	1.187	170.15	0.702	21.26
	Cobalt	Co	5	231.9	1.092	139.43	0.551	17.42
	Silver	Ag	4.7	257.2	0.962	110.75	0.447	13.84
	Copper	Cu	4.65	302.0	0.826	92.52	0.371	11.56
	Aluminum	Al	4.4	365.0	0.695	70.92	0.279	8.86
	Molybdenum	Mo	4.2	421.8	0.601	57.25	0.226	2.82
n-TiO2/p-Cu2O	Platinum	Pt	5.6	280.0	0.977	191.46	0.699	23.93
	Nickel	Ni	5.15	298.9	0.899	162.53	0.605	20.31
	Gold	Au	5.1	324.8	0.832	137.62	0.591	17.21
	Cobalt	Co	5	358.9	0.753	113.33	0.419	14.16
	Silver	Ag	4.7	374.6	0.707	107.21	0.404	13.41
	Copper	Cu	4.65	466.8	0.604	79.92	0.283	9.99
	Aluminum	Al	4.4	560.9	0.515	58.61	0.202	7.32
	Molybdenum	Mo	4.2	606.2	0.419	27.32	0.107	3.41

4. Conclusions

The two devices n-TiO_2/p-CuO and n-TiO_2/p-Cu_2O were successfully synthesized. Different back contact electrodes (Pt, Ni, Au, Co, Ag, Cu, Al, and Mo) were chosen to understand the role played in regulating the advantages of the two fabricated devices. ITO layer was a front contact electrode with a high working function. The optical and structural characteristics showed the superiority of the fabricated device n-TiO_2/p-CuO over the fabricated device n-TiO_2/p-Cu_2O. It is worth noting here that the circuit opening voltage of the n-TiO_2/p-Cu_2O solar cell is lower than the circuit opening voltage of the n-TiO^2/p-CuO solar cell. This is due to the higher optical gap energy of Cu2O (2.18 eV) compared to CuO (1.77 eV). Therefore, we can say that the use of the fabricated device n-TiO_2/p-CuO and the follow-up of research studies to elucidate more of its advantages will positively affect the future of the PV applications. The current study proved the pivotal role that the contact electrodes play and the work function in controlling the properties of solar cells. Since platinum has the highest work function and molybdenum has the lowest work function, the Schottky barrier is higher in platinum, Pt, and lowers in molybdenum, Mo, in the electrodes used in our current study. For this reason, we recommend carefully choosing the contact electrodes based on the ohmic nature of the electrodes and the high work function.

References

[1] S. Hussain, C. Cao, Z. Usman, Z. Chen, G. Nabi, W.S. Khan, Z. Ali, F.K. Butt, T. Mahmood, " Fabrication and photovoltaic characteristics of Cu_2O/TiO_2 thin film heterojunction solar cell," Thin Solid Films 522: 430–434, 2012.

[2] M. Pavan, S. Rühle, A. Ginsburg, D.A. Keller, H. N. Barad, M. Sberna Paolo, D. Nunes, R. Martins, A.Y. Anderson, A. Zaban, E. Fortunato," TiO_2/Cu_2O all-oxide heterojunction solar cells produced by spray pyrolysis," Sol. Energy Mater Sol. Cells 132: 549–556, 2015.

[3] R. Jose, V. Thavasi, S. Ramakrishna, "Metal oxides for dye sensitized solar cells," J. Am. Ceram. Soc. 92: 289–301, 2009.

[4] M. Ichimura, and Y. Kato, "Fabrication of TiO_2/Cu_2O heterojunction solar cells by electrophoretic deposition and electrodeposition," Mater. Sci. Semicond. Process, 16: 1538–1541, 2013.

[5] N. Ueda, H. Maeda, H. Hosono, H. Kawazoe, "Band-gap widening of CdO thin films," Journal of applied Physics, 84(11): 6174-6177, 1998.

[6] H. Liu, X. Zhang, L. Li, Y. X. Wang, K. H Gao, Z. Q. Li, X. X. Zhang, "Role of point defects in room-temperature ferromagnetism of Cr-doped ZnO," Applied physics letters, 91(7): 072511, 2007.

[7] H. Zhu, F. Zhao, L. Pan, Y. Zhang, C. Fan, Y. Zhang, J. Q. Xiao, "Structural and magnetic properties of Mn-doped CuO thin films," Journal of applied physics, 101(9): 09H111, 2007.

[8] A. E. Rakhshani, "Preparation, characteristics and photovoltaic properties of cuprous oxide—a review," Solid-State Electronics, 29(1): 7-17, 1986.

[9] W. Siripala, L. D. R. D. Perera, K. T. L. De Silva, J. K. D. S. Jayanetti, I. M. Dharmadasa, "Study of annealing effects of cuprous oxide grown by electrodeposition technique," Solar Energy Materials and Solar Cells, 44(3): 251-260, 1996.

[10] C. S. Ray, "Preparation of copper oxide thin film by the sol–gel-like dip technique and study of their structural and optical properties," Solar energy materials and solar cells, 68(3): 307-312, 2001.

[11] J. F. Pierson, A. Thobor-Keck, A. Billard, "Cuprite, paramelaconite and tenorite films deposited by reactive magnetron sputtering," Applied surface science, 210(3): 359-367, 2003.

[12] A. Chen, G. Yang, H. Long, F. Li, Y. Li, P. Lu, "Nonlinear optical properties of laser deposited CuO thin films, " Thin Solid Films, 517(15): 4277-4280, 2009.

[13] A. Chen, G. Yang, H. Long, P. Lu, W. Zhang, H. Wang, "Optical limiting properties in copper oxide thin films under a high-repetition-rate femtosecond laser," Materials letters, 91: 319-322, 2013.

[14] D. S. Murali, S. Kumar, R. J. Choudhary, R. J. Wadikarx, M. K. Jain, A. Subrahmanyam, "Synthesis of Cu_2O from CuO thin films: Optical and electrical properties," AIP advances, 5(4): 047143, 2015.

[15] S. Nandy, A. Banerjee E. Fortunato, R. Martins, "A review on Cu_2O and CuI-based p-type semiconducting transparent oxide materials: promising candidates for new generation oxide based electronics," Reviews in Advanced Sciences and Engineering, 2(4): 273-304, 2013.

[16] P. Pattanasattayavong, S. Thomas, G. Adamopoulos, M. A. McLachlan, T. D. Anthopoulos, "p-channel thin-film transistors based on spray-coated Cu2O films," Applied Physics Letters, 102(16): 163505, 2013.

[17] B. Balamurugan, and B. R. Mehta, "Optical and structural properties of nanocrystalline copper oxide thin films prepared by activated reactive evaporation," Thin solid films, 396(1): 90-96, 2001.

[18] L. B. Chen, N. Lu, C. M. Xu, H. C. Yu, T. H. Wang, "Electrochemical performance of polycrystalline CuO nanowires as anode material for Li ion batteries," Electrochimica Acta, 54(17): 4198-4201, 2009.

[19] Y. W. Zhu, T. Yu, F. C. Cheong, X. J. Xu, C. T. Lim, V. B. C. Tan, C. H. Sow, "Large-scale synthesis and field emission properties of vertically oriented CuO nanowire films," Nanotechnology, 16(1): 88, 2004.

[20] S. Saito, M. Miyayama, K. Koumoto, H.Yanagida, "Gas sensing characteristics of porous ZnO and Pt/ZnO ceramics," Journal of the American Ceramic Society, 68(1): 40-43, 1985.

[21] E. Traversa, "Intelligent ceramic materials for chemical sensors," Journal of intelligent material systems and structures, 6(6): 860-869, 1995.

[22] T. Ghodselahi, M. A. Vesaghi, A. Shafiekhani, A. Baghizadeh, M. Lameii, "XPS study of the Cu@ Cu_2O core-shell nanoparticles," Applied Surface Science, 255(5): 2730-2734, 2008.

[23] B. K. Meyer, A. Polity, D. Reppin, M. Becker, P. Hering, P. J. Klar, C. Ronning, "Binary copper oxide semiconductors: From materials towards devices," physica status solidi (b), 249(8): 1487-1509, 2012.

[24] J. Sohn, S. H.Song, D. W. Nam, I. T. Cho, E. S. Cho, J. H. Lee, H. I. Kwon, "Effects of vacuum annealing on the optical and electrical properties of p-type copper-oxide thin-film transistors," Semiconductor science and technology, 28(1): 015005, 2012.

[25] R. Etefagh, E. Azhir, N. Shahtahmasebi, "Synthesis of CuO nanoparticles and fabrication of nanostructural layer biosensors for detecting Aspergillusniger fungi," ScientiaIranica, 20(3): 1055-1058, 2013.

[26] S. G. Rejith, and C. Krishnan, "Optical, thermal and magnetic studies on zinc-doped copper oxide nanoparticles," Materials Letters, 106: 87-89, 2013.

[27] A. O. Musa, T. Akomolafe, M. J. Carter. "Production of cuprous oxide, a solar cell material, by thermal oxidation and a study of its physical and electrical properties," Solar Energy Materials and Solar Cells, 51(3-4): 305-316, 1998.

[28] Y. Hames, and S. Eren San, "CdO/Cu_2O solar cells by chemical deposition," Solar Energy, 77(3): 291-294, 2004.

[29] A. A. Ogwu, E. Bouquerel, O. Ademosu, S. Moh, E. Crossan, F. Placido, "An investigation of the surface energy and optical transmittance of copper oxide thin films prepared by reactive magnetron sputtering," ActaMaterialia, 53(19): 5151-5159, 2005.

[30] M. Ivill, M. E.Overberg, C. R. Abernathy, D. P. Norton, A. F.Hebard, N. Theodoropoulou, J. D. Budai, "Properties of Mn-doped Cu_2O semiconducting thin films grown by pulsed-laser deposition," Solid-State Electronics, 47(12): 2215-2220, 2003.

[31] K. Santra, C. K. Sarkar, M. K. Mukherjee, B. Ghosh, "Copper oxide thin films grown by plasma evaporation method," Thin solid films, 213(2): 226-229, 1992.

[32] R. P. Wijesundara, L. D. R. D.Perera, K. D. Jayasuriya, W. Siripala, K. T. L. De Silva, A. P. Samantilleke, I. M. Dharmadasa, "Sulphidation of electrodeposited cuprous oxide thin films for photovoltaic applications, " Solar energy materials and solar cells, 61(3): 277-286, 2000.

[33] T. Mahalingam, J. S. P. Chitra, J. P. Chu, P. J. Sebastian, "Preparation and microstructural studies of electrodeposited Cu_2O thin films," Materials letters, 58(11): 1802-1807, 2004.

[34] Y. Tang, Z. Chen, Z. Jia, L. Zhang, J. Li, "Electrodeposition and characterization of nanocrystalline cuprous oxide thin films on TiO_2 films," Materials letters, 59(4): 434-438, 2005.

[35] R. P. Wijesundera, M. Hidaka, K. Koga, M. Sakai, W. Siripala, "Growth and characterisation of potentiostatically electrodeposited Cu_2O and Cu thin films," Thin solid films, 500(1-2): 241-246, 2006.

[36] S. K. Ravi, W. Sun, D. K. Nandakumar, Y. Zhang, S. C. Tan, "Optical manipulation of work function contrasts on metal thin films," Science advances, 4(3): 6050, 2018.

[37] R. R. Prabhu, A. C. Saritha, M. R. Shijeesh, M. K. Jayaraj, "Fabrication of p-CuO/n-ZnO heterojunction diode via sol-gel spin coating technique," Materials Science and Engineering: B, 220: 82-90, 2017.

[38] A. Tombak, M. Benhaliliba, Y. S. Ocak, T. Kiliçoglu, "The novel transparent sputtered p-type CuO thin films and Ag/p-CuO/n-Si Schottky diode applications." Results in Physics, 5: 314-321, 2015.

[39] J. Y. Zheng, G. Song, C. W. Kim, Y. S. Kang, "Facile preparation of p-CuO and p-CuO/n-CuWO4 junction thin films and their photoelectrochemical properties," Electrochimica acta, 69: 340-344, 2012.

[40] I. M. Musa, and Y. Abdu, "Fabrication of p-Cu_2O/n-Cu_2O for Photovoltaic Applications," Journal of the Nigerian Association of Mathematical Physics, 33: 271-276, 2016.

[41] M. Izaki, T. Shinagawa, K. T. Mizuno, Y. Ida, M. Inaba, A. Tasaka, "Electrochemically constructed p-Cu_2O/n-ZnOheterojunction diode for photovoltaic device," Journal of Physics D: Applied Physics, 40(11): 3326, 2007.

[42] J. Wu, P. Huang, H. Fan, G. Wang, W. Liu, "Metal–Organic Framework-Derived p-Cu_2O/n-Ce-Fe_2O_3Heterojunction Nanorod Photoanode Coupling with a FeOOH Cocatalyst for High-Performance Photoelectrochemical Water Oxidation," ACS Applied Materials & Interfaces, 12(27): 30304-30312, 2020.

[43] M. Ahmed, A. Bakry, A. Qasem, H. Dalir, "The main role of thermal annealing in controlling the structural and optical properties of ITO thin film layer," Optical Materials, 113: 110866, 2021.

[44] E. R. Shaaban, M. Y. Hassaan, M. G. Moustafa, A. Qasem, G. A. Ali, "Optical constants, dispersion parameters and non-linearity of different thickness of $As_{40}S_{45}Se_{15}$ thin films for optoelectronic applications," Optik, 186: 275-287, 2019.

[45] Z. A. Alrowaili, M. M. Soraya, T. A. Alsultani, A. Qasem, E. R. Shaaban, M. Ezzeldien. "Sn-induced changes in the structure and optical properties of amorphous As–Se–Sn thin films for optical devices," Applied Physics A, 127(2): 1-11, 2021.

[46] M. Alzaid, A. Qasem, E. R. Shaaban, N. M. A. Hadia. "Extraction of thickness, linear and nonlinear optical parameters of $Ge_{20+x}Se_{80-x}$ thin films at normal and slightly inclined light for optoelectronic devices," Optical Materials, 110: 110539, 2020.

[47] A. Qasem, M. Y. Hassaan, M. G. Moustafa, M.A. S. Hammam, H. Y. Zahran, I. S. Yahia, E. R. Shaaban. "Optical and electronic properties for As-60 at.% S uniform thickness of thin films: Influence of Se content, " Optical Materials, 109 (2020): 110257.

[48] H. I. Elsaeedy, A. Qasem, H. A. Yakout, M. Mahmoud. "The pivotal role of TiO_2 layer thickness in optimizing the performance of TiO_2/P-Si solar cell." Journal of Alloys and Compounds 867: 159150, 2021.

[49] R. Tang, X. Fu, C. Ning, "Accurate electron affinity of Ti and fine structures of its anions," J. Chem. Phys., 149(13): 134304, 2018.

[50] W. Chaibi, R. J.Peláez, C. Blondel, C. Drag, C. Delsart, "Effect of a magnetic field in photodetachment microscopy," Eur. Phys. J. D, 58 (1): 29-37, 2010.

[51] R. C. Bilodeau, M. Scheer, H. K. Haugen, "Infrared laser photodetachment of transition metal negative ions: studies on, and," Journal of Physics B: Atomic, Molecular and Optical Physics, 31(17): 3885, 1998.

[52] A. S. Hassanien, I. Sharma, "Band-gap engineering, conduction and valence band positions of thermally evaporated amorphous $Ge_{15-x}Sb_xSe_{50}Te_{35}$ thin films: Influences of Sb upon some optical characterizations and physical parameters,: J. Alloys Compd., 798:750-763, 2019.

[53] S. G. Bratsch, and J. J. Lagowski, "Predicted stabilities of monatomic anions in water and liquid ammonia at 298.15 K," Polyhedron, 5 (11): 1763-1770, 1986.

[54] N. Ryo, "Extraction of the Schottky parameters in metal-semiconductor-metal diodes from a single current-voltage measurement," Journal of Applied Physics, 116: 184505, 2014.

[55] G. Winter, H. Heckmann, P. Haisch, W. Eberhardt, M. Hanack, L. Lüer, H. J. Egelhaaf, D. Oelkrug, "Study of substituent effects on the photoconductivity of soluble 2, (3)-and 1, (4)-substituted phthalocyaninato and naphthalocyaninatotitanium (IV) oxides," Journal of the American Chemical Society, 120 (45): 11663-11673, 1998.

[56] A. Mellit, "Artificial intelligence based-modeling for sizing of a stand-alone photovoltaic power system: Proposition for a new model using Neuro-Fuzzy system (ANFIS)," 3rd International IEEE Conference Intelligent Systems. IEEE, 2006.

[57] S. Meir, C. Stephanos, T. H. Geballe, J. Mannhart, "Highly-efficient thermo electronic conversion of solar energy and heat into electric power," J. Renew. Sustain. Energy, 5(4): 043127, 2013.

[58] L. Jin, G. Sirigu, X. Tong, A. Camellini, A. Parisini, G. Nicotra, A. Vomiero, "Engineering interfacial structure in “Giant” PbS/CdS quantum dots for photoelectrochemical solar energy conversion," Nano Energy, 30: 531-541, 2016.

[59] N. Das, D. Chandrasekar, M. M. K. Khan, "Light Reflection Loss Reduction by Nano-Structured Gratings for Highly Efficient Next-Generation GaAs Solar Cells," Energies, 13(16): 4198, 2020.

[60] S. Shao, and M.A. Loi, "The role of the interfaces in perovskite solar cells," Advanced Materials Interfaces, 7(1): 1901469, 2020.

[61] S. Solak, P. W.M. Blom, G. A. H. Wetzelaer, "Effect of non-ohmic contacts on the light-intensity dependence of the open-circuit voltage in organic solar cells," Applied Physics Letters, 109(5): 053302, 2016.

[62] F. Yan, Y. Wang, J. Zhang, Z. Lin, J. Zheng, F. Huang, "Schottky or ohmic metal–semiconductor contact: influence on photocatalytic efficiency of Ag/ZnO and Pt/ZnO model systems," Chem. Sus. Chem., 7(1): 101-104, 2014.

[63] P. Cusumano, C. Arnone, M. A. Giambra, A. Parisi, "Donor/acceptor heterojunction organic solar cells," Electronics, 9(1): 70, 2020.

[64] M. Zhang, H. Wang, C. W. Tang, "Effect of the highest occupied molecular orbital energy level offset on organic heterojunction photovoltaic cells," Applied physics letters, 97(14): 143503, 2010.

[65] U. Dutta, and P. Chatterjee, "The open circuit voltage in amorphous silicon p-i-n solar cells and its relationship to material, device and dark diode parameters," Journal of applied physics, 96(4): 2261-2271, 2004.

[66] J. Guo, J. Bouwmeester, E. Gill, "In-orbit results of Delfi-n3Xt: Lessons learned and move forward," Acta Astronautica, 121: 39-50, 2016.

[67] H. C. Barshilia, N. Selvakumar, K. S.Rajam, D. V. S. Rao, K. Muraleedharan, A. Biswas, "TiAlN⁄ TiAlON⁄ Si_3N_4 tandem absorber for high temperature solar selective applications," Applied Physics Letters, 89(19): 191909, 2006.

مقالة بحثية

دراسة الخصائص التركيبية والبصرية و الكهروضوئية للخلايا الشمسية المصنعة من $n\text{-}TiO_2/p\text{-}CuO$ و $n\text{-}TiO_2/p\text{-}Cu_2O$ عن طريق تغيير أقطاب التوصيل الخلفية

مهدي احمد دبان[1،*] و عمار قاسم الخطيب[2]

[1] قسم الفيزياء، كلية العلوم، جامعة عدن، عدن، ص.ب. 6312، اليمن
[2] قسم الفيزياء، كلية العلوم، جامعة الأزهر، مدينة نصر 11884، القاهرة، مصر

* الباحث الممثّل: مهدي احمد دبان؛ البريد الالكتروني: mehdi.ahmed.scie@aden-univ.net

استلم في: 09 يوليو 2022 / قبل في: 21 يوليو 2022 / نشر في 30 سبتمبر 2022

المُلخّص

تهدف الدراسة إلى مقارنة الخصائص التركيبية والبصرية والخلايا الكهروضوئية لخليتين شمسيتين مصنوعتين من $n\text{-}TiO_2/p\text{-}CuO$ و $n\text{-}TiO_2/p\text{-}Cu_2O$. وتناولت تأثير المعادن المختلفة كأقطاب كهربائية للتوصيل الخلفي على الخصائص الكهروضوئية للخلايا الشمسية المصنعة، وذلك لفهم الدور الذي تلعبه في تنظيم خواص الخلايا الشمسية. كان القطب التوصيل الأمامي في كلا الخليتين عبارة عن طبقة زجاجية مطلية بـ TIO، في حين أن أقطاب الاتصال الخلفية كانت (Mo, Al, Cu, Ag, Co, Au, Ni, and Pt).
أظهرت القياسات الضوئية للأغشية الرقيقة TiO_2 (سُمك 120 نانومتر)، CuO (سُمك 200 نانومتر)، و CuO_2 (سُمك 200 نانومتر)، إن الانتقالات الاليكترونية المسئولة عن عملية الامتصاص هي من النوع المباشر، كما إن قيم طاقة الفجوة الضوئية بناءً على معادلة Tauc تكون 3.24 و 1.77 و 2.18 إلكترون- فولت، على التوالي. كما بينت الخصائص البصرية والهيكلية جودة الخلية الشمسية المصنعة من $n\text{-}TiO_2/p\text{-}CuO$ مقارنة بتلك المُصنَّعة من $n\text{-}TiO_2/p\text{-}Cu_2O$، لذلك متابعة الدراسات البحثية لتوضيح المزيد من مزاياها سيؤثر بشكل إيجابي على مستقبل التطبيقات الكهروضوئية. أثبتت الدراسة الحالية الدور المحوري الذي تلعبه أقطاب التوصيل المعدنية المختلفة في التحكم في خصائص الخلايا الشمسية.

الكلمات المفتاحية: الأغشية الرقيقة، الخواص الضوئية، الخلايا الشمسية *$n\text{-}TiO_2/p\text{-}CuO$* و *$n\text{-}TiO_2/p\text{-}Cu_2$*.

How to cite this article:

M. A. Dabban and A. Qasem, "TUNING THE STRUCTURAL, OPTICAL AND PHOTOVOLTAIC CHARACTERISTICS OF FABRICATED N-TIO2/P-CUO AND N-TIO2/P-CU2O SOLAR CELLS BY CHANGING THE BACK CONTACT ELECTRODES", *Electron. J. Univ. Aden Basic Appl. Sci.*, vol. 3, no. 3, pp. 130-144, Sept. 2022. DOI: https://doi.org/10.47372/ejua-ba.2022.3.178